Journal of Physics: Conference Series **228** (2010) 012056 doi:10.1088/1742-6596/228/1/012056

Numerical studies of the efficiency of resonant relaxation around a massive black hole

Gábor Kupi, Ehud Eilon[1] and Tal Alexander

Faculty of Physics, Weizmann Institute of Science, Rehovot 76100, Israel

E-mail: gabor.kupi@weizmann.ac.il

Abstract. Resonant relaxation (RR) is a rapid relaxation process that operates in the nearly-Keplerian potential near a massive black hole (MBH). RR dominates the dynamics of compact remnants that inspiral into a MBH and emit gravitational waves (extreme mass ratio inspiral events, EMRIs). RR can either increase the EMRI rate, or strongly suppress it, depending on its still poorly-determined efficiency. We use small-scale Newtonian N-body simulations to measure the RR efficiency and to explore its possible dependence on the stellar number density profile around the MBH, and the mass-ratio between the MBH and a star (a single-mass stellar population is assumed). We present a suite of simulations with a range of stellar density profiles and mass-ratios, and measure the mean RR efficiency in the near-Keplerian limit. We do not find a strong dependence on the density profile or the mass-ratio. Our numerical determination of the RR efficiency in the Newtonian, single-mass population approximations, suggests that RR will likely enhance the EMRI rate by a factor of a few over the rates predicted assuming only slow stochastic two-body relaxation.

1. Introduction

Dynamical relaxation processes near MBHs in galactic centers affect the rates of strong stellar interactions with the MBH, such as tidal disruption, tidal dissipation, or gravitational wave (GW) emission (e.g. [1]). These relaxation processes may also be reflected by the dynamical properties of the different stellar populations there [6], as observed in the Galactic Center [5, 7]. Of particular importance, in anticipation of the planned Laser Interferometer Space Antenna (LISA) GW detector, is to understand the role of relaxation in regulating the rate of GW emission events from compact remnants undergoing quasi-periodic EMRI into MBHs.

Two-body relaxation, or non-coherent relaxation (NR), is inherent to any discrete large-N system, due to the cumulative effect of uncorrelated two-body encounters. These cause the orbital energy E and the angular momentum J to change in a random-walk fashion ($\propto \sqrt{t}$) on the typically long NR timescale T_{NR}. In contrast, when the gravitational potential has approximate symmetries that restrict orbital evolution (e.g. fixed ellipses in a Keplerian potential; fixed orbital planes in a spherical potential), the perturbations on a test star are no longer random, but correlated, leading to coherent ($\propto t$) torquing of J on short timescales, while the symmetries hold. Over longer times, this results in resonant relaxation (RR) [10, 9], a rapid random walk of J on the typically short RR timescale $T_{RR} \ll T_{NR}$. RR in a near-Keplerian potential can change both the direction and magnitude of $\mathbf{J}$ ("scalar RR"), thereby driving stars to near-radial

[1] Present address: Israel Aerospace Industries, Ben Gurion International Airport, 70100, Israel

orbits that interact strongly with the MBH. RR in a near-spherical potential can only change the direction of **J** ("vector RR").

RR is particularly relevant in the potential near a MBH, where compact EMRI candidates originate. Hopman and Alexander [6] show that RR dominates EMRI source dynamics. Depending on its still poorly-determined efficiency, RR can either increase the EMRI rate over that predicted assuming NR only, or if too efficient, it can strongly suppress the EMRI rate by throwing the compact remnants into infall (plunge) orbits that emit a single, non-periodic and hard to detect GW burst. The still open questions about the implications of RR for EMRI rates and orbital properties provide a prime motivation for the systematic numerical investigation of RR efficiency presented here. A more detailed treatment of this subject can be found in [4].

2. Theory

2.1. Non-coherent Relaxation (NR)

The NR time for E-relaxation, $T^E_{\rm NR}$, corresponds to the time it takes non-coherent 2-body interactions to change the stellar orbital energy by order of itself, $|\Delta E|\sim E$ (by stellar dynamical definition convention, $E>0$ for a bound orbit). Similarly, the NR time for J-relaxation, $T^J_{\rm NR}$, corresponds to the time it takes the stellar orbital angular momentum to change by order of the circular angular momentum $|\Delta J|\sim J_c$, where near a MBH of mass M, $J_c=GM/\sqrt{2E}$. The E-relaxation timescale can be estimated by considering the rate of gravitational collisions in a system of size R between a test star and N field stars: $T^E_{\rm NR}\sim(M/m)^2P/(N\ln\Lambda)$, where m is the mass of stars, $P=2\pi\sqrt{R^3/GM}$ is the Keplerian period and Λ is the Coulomb logarithm $\ln\Lambda\sim\ln(R/r_{min})$, r_{min} is the minimal impact parameter where the small angle deflection assumption still holds. Near the MBH $\ln\Lambda\sim\ln Q$, where $Q\equiv M/m$.

Rauch and Tremaine [10] (RT96) parametrized the uncertainties in the evolution of the orbital E, J and **J** by a set of numeric coefficients (α_Λ, $\eta_{s,v}$, $\beta_{s,v}$), whose operational definition is tied to the procedure by which they are estimated (left unspecified by RT96). We adopt this notation and estimate these coefficients by the rms change over the stellar population. The NR changes in E, J and **J** (here generally denoted by x) over the dimensionless time-lag $\tau\equiv(t_2-t_1)/P_1$ are thus formally defined as

$$\delta x(\tau) \equiv \left\langle \left(|x_2-x_1|/x_0\right)^2\right\rangle^{1/2} = K(\sqrt{N}/Q)\sqrt{\tau} \qquad (1)$$

where x_0 is E_1 for E and $J_{c,1}$ (angular momentum of circular orbit) for J and **J**. The dimensionless, order-unity constants K are $\alpha\sqrt{\ln\Lambda}$, $\eta_s\sqrt{\ln\Lambda}$ and $\eta_v\sqrt{\ln\Lambda}$ respectively. The exact determination of these constants, which are system-dependent, requires detailed calculations or simulations. The corresponding NR timescales are related to these coefficients by $T^E_{\rm NR}=(M/m)^2P/(N\alpha^2_\Lambda)$, $T^J_{\rm NR}=(M/m)^2P/(N\eta^2_{s\Lambda})$ and $T^{\mathbf{J}}_{\rm NR}=(M/m)^2P/(N\eta^2_{v\Lambda})$.

2.2. Resonant Relaxation (RR)

When the gravitational potential has symmetries that restrict the orbital evolution, for example to fixed ellipses in the potential of a point mass, or to planar annuli in a spherical potential, the perturbations on a test star are no longer random, but correlated. This leads to a coherent changes in **J** on times $P\ll t<t_\omega$, $\Delta\mathbf{J}=\mathbf{T}t$, by the residual torque $|\mathbf{T}|\sim\sqrt{N}Gm/R$ exerted by the N randomly oriented, orbit-averaged mass distributions of the surrounding stars (mass wires for elliptical orbits in a Kepler potential, mass annuli for rosette-like orbits in a spherical potential). The coherence time t_ω is set by deviations from the true symmetry, which lead to a gradual orbital drift and to the randomization of **T**. For example, the enclosed stellar mass leads to non-Keplerian retrograde precession; General Relativity leads to prograde precession. Ultimately, the coherent torques themselves randomize the orbits. The effective coherence time is set by the

shortest de-coherence (quenching) process. The accumulated change over t_ω, $|\Delta\mathbf{J}_\omega| \sim |\mathbf{T}t_\omega|$, then becomes the basic step-size, or mean free path in $\mathbf{J}$-space, for the long-term ($t \gg t_\omega$) random-walk phase ($\propto \sqrt{t}$) of $\mathbf{J}$ by RR . Since this step-size is large, RR can be much faster than NR. The RR timescale $T_{\rm RR}$ is then defined by $|\Delta J|/J_c = (|\Delta J_\omega|/J_c)\sqrt{t/t_\omega} \equiv \sqrt{t/T_{\rm RR}}$. Note that the relaxation of E is not affected by RR because the potential of the system is stationary on the coherence timescale, and so E changes incoherently on all time scales. The torques exerted by elliptical mass wires in a Kepler potential can change both the direction and magnitude of $\mathbf{J}$. In contrast, the torques exerted by planar annuli can only change the direction of $\mathbf{J}$. The long-term random walk $\sqrt{\tau}$ growth continues until $|\Delta\mathbf{J}|/J_c \sim O(1)$, at which point $|\Delta J|/J_c$ and $|\Delta\mathbf{J}|/J_c$ can no longer grow, but $\mathbf{J}$ does continue to change its value randomly.

Here we consider only Newtonian dynamics. The coherence timescale for scalar RR is determined by the time it takes for the orbital apsis to precess by angle $\sim\pi$ due to the potential of the enclosed stellar mass ("mass precession"),

$$t_\omega = t_M = A_M\,(Q/N)\,P\,, \tag{2}$$

where A_M is an $O(1)$ factor reflecting the approximations in this estimate. The coherence timescale for vector RR is determined by the time it takes for the coherent torques to change $|\Delta\mathbf{J}| \sim J_c$

$$t_\omega = t_\phi = A_\phi\left(\sqrt{N}/\mu\right)P \simeq \left[A_\phi Q\Big/\sqrt{N}\right]P\,, \tag{3}$$

where A_ϕ is an $O(1)$ factor, $\mu = Nm/(M+Nm)$ and where the approximate equality is for the Keplerian limit $Nm \ll M$. The RR changes in J and $\mathbf{J}$ during the coherent phase ($\tau < \tau_\omega$) are defined in terms of the rms change in analogy with Eq. (1)

$$\delta J(\tau) = \beta_s\frac{\sqrt{N}}{Q}\tau\,, \quad \delta\mathbf{J}(\tau) = \beta_v\frac{\sqrt{N}}{Q}\tau\,, \tag{4}$$

where the dimensionless coefficients β_s and β_v depend on the parameters of the system and reflect the uncertainties introduced by the various approximations and simplification of this analysis. Accurate determination of their values requires detailed calculations or simulations.

The scalar RR change in J on time-lags $\tau \gg \tau_M$ and the scalar RR timescale are then

$$\delta J(\tau) = \beta_s\sqrt{A_M/Q}\sqrt{\tau}\,, \quad T^J_{\rm RR} = \left[Q/A_M\beta_s^2\right]P\,. \tag{5}$$

The RR efficiency factor $\chi = (\beta_s/\beta_{s,\rm RT96})^2$ defined by [6] for an assumed value $A_M = 1$, expresses how much shorter $T^J_{\rm RR}$ is relative to the value estimated by RT96. Scalar RR is faster than NR by a factor $T^J_{\rm NR}/T^J_{\rm RR} \propto (M/m)/N\ln\Lambda$. Similarly, the vector RR change in $\mathbf{J}$ on time-lags $\tau \gg \tau_\phi$ in the Keplerian limit and the vector RR timescale are

$$\delta\mathbf{J}(\tau) = \beta_v\sqrt{A_\phi\sqrt{N}/Q}\sqrt{\tau}\,, \quad T^{\mathbf{J}}_{\rm RR} = \left[Q\Big/\sqrt{N}A_\phi\beta_v^2\right]P\,. \tag{6}$$

3. Simulations

Our N-body code uses a 5th order Runge-Kutta integrator without gravity softening. The time steps were chosen to conserve total energy at the level of $|\Delta E_{\rm tot}|/E_{\rm tot} \sim O(10^{-5}) - O(10^{-8})$, well below the NR energy changes expected in the simulations.

To simulate RR reliably, the N-body code must maximize angular momentum conservation and minimize numerical RR quenching, which can be caused by numerical precession of the apsis, which changes the torque, or to a lesser degree by a drift in the orbital period (equivalently, the

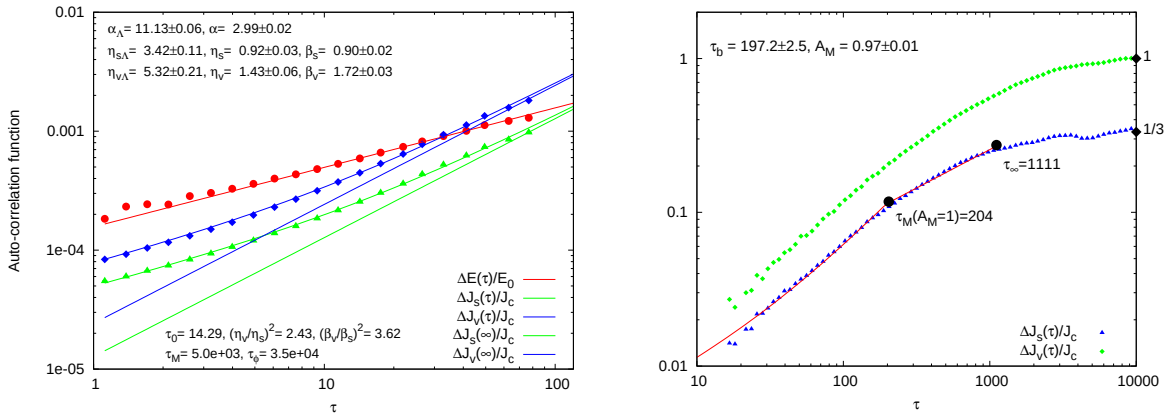

Figure 1. Left: The measured (points) and fitted (lines) correlation curves for δE (top line), δJ (bottom line) and $\delta \mathbf{J}$ (middle line) in a $Q=10^6$, $\gamma=1.5$ simulation with $N=200$ particles. The points are the results of the N-body simulation, the thick lines are the predicted theoretical curves; the thin straight lines show the asymptotic linear behavior. The best fit coefficients and related quantities are also listed. **Right**: The long-term scalar RR (bottom curve) and vector RR (top curve) in a $Q=10^4$ simulation with $N=49$ particles and $\gamma=1$ density profile. The mass-precession timescale τ_M is calculated from Eq. (2) with the assumption that $A_M=1$ (verified here, see text). The saturation timescale of scalar RR, τ_∞, is defined by $\left(\tau_\infty/\tau^J_{RR}\right)^{1/2}=1/3$.

energy), which changes the moment of inertia of the "mass wire". We estimated these numerical drifts by integrating, over many orbits, a highly eccentric 2-body system ($e=0.99995$, $Q=3\times10^6$), since most of the numerical errors accumulate at periapse, where the acceleration is largest. We tracked the change in the period, $\Delta P=(P-P_0)/P_0$, in the angular momentum $\Delta\mathbf{J}=|\mathbf{J}-\mathbf{J}_0|/J_0$ and in the direction of the apsis $\Delta\hat{\mathbf{e}}=|\hat{\mathbf{e}}-\hat{\mathbf{e}}_0|/|\hat{\mathbf{e}}_0|$, where $\hat{\mathbf{e}}$ is the normalized Runge-Lenz vector. We find that after $\tau_{\rm sim}=4.5\times10^4$, $\Delta P\sim8\times10^{-5}$, $\Delta\mathbf{J}\sim3\times10^{-4}$ and $\Delta\hat{\mathbf{e}}\sim9\times10^{-8}$, which correspond to drift timescales of $\tau_{\Delta P}\sim(\pi/\Delta P)\tau_{\rm sim}=2\times10^9$, $\tau_{\Delta\mathbf{J}}\sim5\times10^8$ and $\tau_{\Delta\hat{\mathbf{e}}}\sim3\times10^{12}$. These are many orders of magnitude longer than our longest simulations, and can therefore be safely neglected.

We carried out two sets of Newtonian simulations. The first, designed to study the short-term behavior of RR ($\tau_{\rm sim}<\tau_M$) and to measure NR and RR parameters α, $\eta_{s,v}$ and $\beta_{s,v}$, consisted of 200 particles (including the MBH as a fixed particle in the origin of the coordinate system). The initial orbital semi-major axes were randomly drawn from a $\rho(a)da\propto a^{2-\gamma}da$ distribution for $\gamma=1$, 1.5, 1.75, for a in the range $(0,1/2)$, with eccentricities drawn from a thermal $\rho(e)de=2ede$ distribution, with random phases, orbital orientations and isotropic velocities. This distribution corresponds approximately to a $r^{-\gamma}$ number density distribution with an outer cutoff at radius $r=R=1$ from the MBH (in dimensionless units where $G=1$, $M+Nm=1$). We made $n_{\rm sim}=114$ simulations in this set.

The second set of simulations was designed to study the long term behavior of RR ($\tau\gg\tau_\phi$), the transition from the coherent RR phase to the random-walk phase, and the asymptotic saturation limits. Due to the high computational load, this set ($n_{\rm sim}=7$) was limited to a relatively small mass ratios, $Q\leq10^4$, smaller number of particles, ($50\leq N\leq200$) and flat cusps with $\gamma=1$, where time-consuming close star-star interactions are rarer.

4. Results

The results of a typical Keplerian simulation are shown in Fig. 1L. Note that in such a potential, vector RR measures the combined change in the magnitude *and* direction of the

Table 1. Measured NR and RR coefficients [a].

γ	Q	$n_{\rm sim}$	$\bar{\alpha}_\Lambda$	$\bar{\eta}_{s\Lambda}$	$\bar{\eta}_{v\Lambda}$	$\bar{\beta}_s$	$\bar{\beta}_v$
1	10^6	12	10.48±0.43	4.58±0.38	7.31±0.61	1.14±0.07	1.95±0.08
1	10^7	12	9.37±0.32	4.18±0.26	6.69±0.46	1.13±0.07	1.98±0.10
1	10^8	12	10.27±0.36	4.26±0.22	7.02±0.47	1.13±0.06	1.89±0.08
1.5	10^6	13	12.61±0.90	4.12±0.48	6.65±0.61	1.00±0.05	1.77±0.07
1.5	10^7	12	11.35±0.46	4.09±0.35	6.58±0.57	1.05±0.06	1.86±0.07
1.5	10^8	12	10.51 ± 0.51	3.99±0.21	6.57±0.49	1.09±0.07	1.92±0.09
1.75	10^6	14	12.06±0.54	3.97±0.35	6.50±0.48	0.95±0.06	1.68±0.06
1.75	10^7	12	12.29±0.43	3.39 ± 0.14	5.29±0.18	0.99±0.07	1.75±0.09
1.75	10^8	15	11.90±0.43	3.89±0.39	6.20±0.52	1.01±0.05	1.73±0.05
Grand average[b]		114	$\langle\alpha\rangle$ 2.82±0.05	$\langle\eta_s\rangle$ 1.01±0.03	$\langle\eta_v\rangle$ 1.64±0.04	$\langle\beta_s\rangle$ 1.05±0.02	$\langle\beta_v\rangle$ 1.83±0.03

[a] The quoted errors are the errors on the mean (the sample rms is $\sqrt{n_{\rm sim}}$ times larger).
[b] $\langle\alpha\rangle = \left\langle\alpha_\Lambda/\sqrt{\ln\Lambda}\right\rangle$, $\langle\eta_{s,v}\rangle = \left\langle\eta_{s,v\Lambda}/\sqrt{\ln\Lambda}\right\rangle$ over all simulations for $\Lambda = Q$.

angular momentum vector. The numerical prefactors $\eta_{s\Lambda}$ and β_s are obtained by fitting the δJ curve to the function $\delta J = (\sqrt{N}/Q)\sqrt{\eta_{s\Lambda}^2\tau + \beta_s^2\tau^2}$. Note that NR dominates the evolution at early times, $\tau < \tau_0 \equiv \eta_{s,v\Lambda}^2/\beta_{s,v}^2$. A similar procedure is used to obtain $\eta_{v,\Lambda}$ and β_v.

We summarize our results in table (1). The coefficients α_Λ and $\eta_{s,v\Lambda}$ do not directly express the intrinsic properties of NR, since they should vary as $\sqrt{\ln\Lambda} \simeq \sqrt{\ln Q} \simeq 4(1\pm0.07)$ over the Q-range of our models. This small fractional difference and the relatively low statistics of our simulation suite may explain why we do not detect a clear Q-dependence in these quantities. Since we do not see a dependence on Q, and the γ dependence seems weak (α_Λ shows hints of an increase with γ, and η and β of a decrease with γ), we adopt as the best fit estimates of the values of α, $\eta_{s,v}$ and $\beta_{s,v}$ their grand average over all the simulations.

To explore the long-term behavior of the system, verify that the short-timescale coherent torquing phase leads to long-term relaxation and to estimate the coefficients that enter the coherence timescales, we also conducted several very long simulations ($\tau \sim 10^4 \gg \tau_\phi$). The resulting RR correlation scalar curves clearly display a first clear detection of a transition at the mass precession coherence time $\tau_M = A_M Q/N$ (Eq. 2) from the asymptotically $\propto \tau$ coherent RR phase to the $\propto \sqrt{\tau}$ RR relaxation phase (Fig 1R). The mean best-fit estimate over 7 long time-scale simulations is $A_M = 0.99\pm0.06$, where the error is dominated by the simulation to simulation scatter. The vector RR curve does not display a coherent rise beyond τ_M, since by its definition it includes a scalar component, and neither a distinct random-walk phase beyond τ_ϕ, since the transition to the asymptotic saturation limit occurs soon after, at $\tau \gtrsim \tau_\phi$. This non-trivial behavior makes it harder to quantify and measure A_ϕ by a fit to the correlation curve, and we do not attempt it here.

Our analytical calculations predict that on very long time-lags, the correlation curves saturate to $\delta J \to 1/3$ and $\delta\mathbf{J} \to 1$ [4]. These limits can be seen in Fig. (1R).

5. Implications for gravitational wave source dynamics

We conclude the discussion of our results by briefly considering the implications of this revised value of β_s for EMRI rates. [6] assumed $A_M = 1$, parametrized the RR efficiency by a factor $\chi = [\beta_s/\beta_{s,\rm RT96}]^2$, and derived the χ dependence of the branching ratio of the EMRI and infall (plunge) rates (Fig. 2). The RT96 value $\chi = 1$ happens to lie very close to the maximum of the RR-accelerated EMRI rate. We confirm here that $A_M = 0.99 \pm 0.06$ and find $\beta_s/\beta_{s,\rm RT96} = 1.98 \pm 0.04$, which corresponds to a factor 4.9 increase in the EMRI rate compared to that estimated for NR only, but is a factor ~ 1.5 smaller than implied by the RT96 value, because the higher RR efficiency leads to a higher plunge rate at the expense of the inspiral rate.

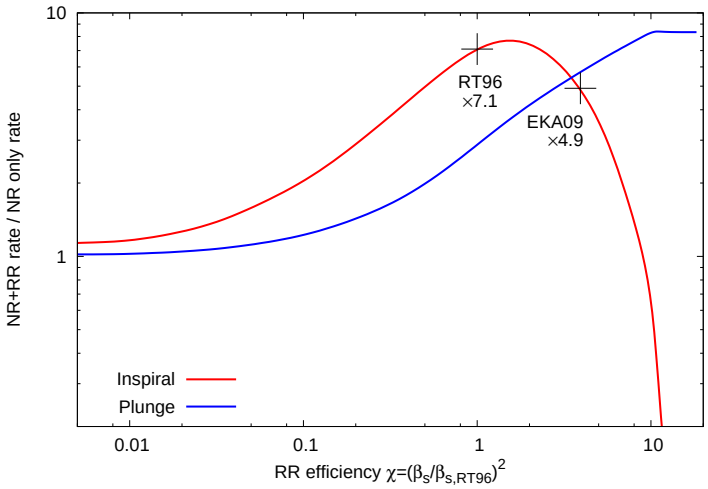

Figure 2. The change in the EMRI and plunge rates relative to that predicted assuming only NR, as function of the RR efficiency χ (Adapted from [6], Fig. 5). The RT96 estimate of β_s ($\chi = 1$) predicts an increase of $\times 7.1$ in the EMRI rate due to RR, close to the maximum. Our new ([4], EKA09) higher measured RR efficiency ($\chi = 3.9$) predicts an increase of only $\times 4.9$ in the EMRI rate, and a higher plunge rate.

6. Summary

We characterized and measured the mean efficiency coefficients of NR ($\alpha_\Lambda, \eta_{s,\Lambda}, \eta_{v,\Lambda}$) and RR ($\beta_s, \beta_v$) in Newtonian N-body simulations of isotropic, thermal, near-Keplerian stellar cusps around a MBH. We measured these coefficients in a large suite of small scale N-body simulations with different stellar density distributions and MBH/star mass ratios. We do not find strong trends in the values of these coefficients as function of the system properties. This may require better statistics. We identified an early phase of NR-dominated relaxation that precedes the coherent RR phase. We carried out several long-term simulations and robustly detected, for the first time, the transition from the coherent to the random walk phase of RR, measured the efficiency of RR, and observed the asymptotic limits of the angular momentum correlation curves. Our measured RR efficiency suggests that RR increases the EMRI rate by a factor of ~ 5 above what is predicted for NR only.

Our measured RR efficiency is broadly consistent with that suggested by the analysis of the dynamical properties of the different stellar populations in the Galactic Center, which indicates an unusually rapid randomization of the stellar orbits [6, 8], and with the warping of the maser disk of NGC 4258, if interpreted as due to RR [3].

References

[1] Alexander, T. 2005, Phys. Rep., 419, 65
[2] Bahcall, J. N. & Wolf, R. A. 1977, ApJ, 216, 883
[3] Bregman, M. & Alexander, T. 2009, ApJ, 700, L192
[4] Eilon, E., Kupi G. & Alexander, T., 2009, ApJ, 698, 641
[5] Genzel, R., Pichon, C., Eckart, A., Gerhard, O. E., & Ott, T. 2000, MNRAS, 317, 348
[6] Hopman, C. & Alexander, T. 2006, ApJ, 645, 1152
[7] Paumard, T. et al. 2006, ApJ, 643, 1011
[8] Perets, H. B., Gualandris, A., Kupi, G., Merritt, D. & Alexander, T., 2009, ApJ, 702, 884
[9] Rauch, K. P. & Ingalls, B. 1998, MNRAS, 299, 1231
[10] Rauch, K. P. & Tremaine, S. 1996, New Astronomy, 1, 149